

Increasing membrane permeability by increasing the polymer crystallinity: the unique case of polythiophenes

Mikael Monga Mulunda^{1,2}, Cédric van Goethem², Rhea Verbeke², Tönjes Koschine², Michael Wübbenhorst³, Zidan Zhang⁴, Erik Nies⁴, Marcel Dickmann⁵, Werner Egger⁶, Ivo F.J. Vankelecom², and Guy Koeckelberghs^{1*}.

¹Laboratory for Polymer Synthesis, KU Leuven, Celestijnenlaan 200F, 3001 Heverlee (Leuven), Belgium

²Centre for Surface Chemistry and Catalysis, KU Leuven, Celestijnenlaan 200F, 3001 Heverlee (Leuven), Belgium

³Laboratory for Soft Matter and Biophysics, KU Leuven, Celestijnenlaan 200D, 3001 Heverlee (Leuven), Belgium

⁴Laboratory for physical chemistry of polymer materials, KU Leuven, Celestijnenlaan 200F, 3001 Heverlee (Leuven), Belgium

⁵Heinz Maier-Leibnitz Zentrum (MLZ) and Physik Department E21, Technische Universität München, Lichtenbergstraße 1, 85748 Garching, Germany

⁶Institut für Angewandte Physik und Messtechnik, Universität der Bundeswehr München, 85577 Neubiberg, Germany

Keywords: rr-P3ATs, supramolecular organization, gas separation membranes

Abstract: It is generally accepted in membrane technology that crystalline zones in polymeric membranes do not contribute to transport of liquids nor gases. In current study, poly(3-alkylthiophene)s (P3ATs), i.e. homopolymers and random copolymers, were synthesized to study the influence of the supramolecular organization on membrane gas separations. The monomers were polymerized via KCTCP and GPC analysis shows that the polymers have a narrow dispersity. DSC analysis of the polymers reveals that the homopolymers, in contrast to

the copolymers, crystallized, confirming their higher degree of supramolecular organization. This was supported by UV-vis absorption spectra of the polymer films, where a red-shift and a characteristic shoulder absorption peak around 600 nm were observed for the homopolymers, while absent for the copolymers. More surprisingly, the homopolymers were found to be two orders of magnitude more permeable to CO₂ than the copolymers and also more selective.

INTRODUCTION

Research on polymeric membranes for gas separations has attracted continuously increasing interest, owing to their economic and environmental advantages over traditional separation processes.^{1,2} Polymeric membranes can be used for the purification of a wide variety of gas mixtures, e.g., upgrading of methane from CO₂/CH₄ mixtures (natural gas and biogas), enrichment of oxygen from N₂/O₂ mixtures (air), removal of carbon dioxide from flue gas (CO₂/N₂) and many more. The membrane performance is primarily determined by two properties: the permeability (P) on one hand, and the selectivity (α) on the other.³ The permeability can be considered the reverse of the resistance for the transport of a given gas across the membrane and is generally expressed in Barrer (1 Barrer = 10⁻¹⁰cm³(STP)cm cm⁻²s⁻¹ cmHg⁻¹); while the selectivity indicates the separation capacity of the membrane toward penetrant gas molecules.

For industrial applications, a membrane should mainly possess both high permeability and good selectivity.² Only a very limited number of polymer types has been commercialized as membrane materials for gas separations.^{1,4} To overcome this, a great deal of effort has been focused on investigating new polymer structures which can fulfill the above requirements. Among them, conjugated polymers (CPs) have been explored as promising gas separation

materials.⁵⁻⁷ Polyaniline (PANI),^{8,9} polypyrrole (PPy) and regio-irregular poly(3-alkylthiophene)s (ri-P3ATs)^{10,11} have all been investigated. Recently, our group has studied for the first time regio-regular (rr) rr-P3ATs with improved performance thanks to better control of the supramolecular structure.¹² However, it should be mentioned that relatively little is known about the fundamental relationship between CP structures and the membrane performances.⁷ Further investigations are needed to assess this relationship if one wants to optimize the gas separation properties of CPs.

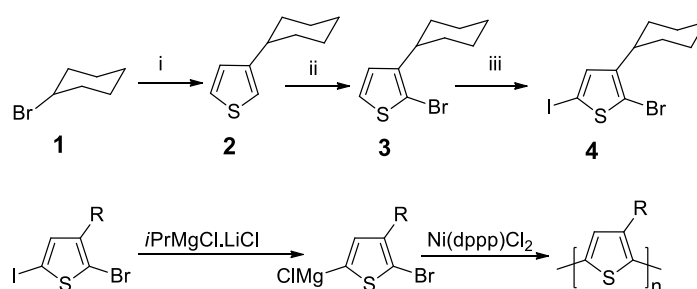
Following the strategy pursued in our previous studies,¹² in the current work two types of rr-P3ATs, homopolymers and random copolymers, were synthesized with the aim to evaluate the influence of the supramolecular organization and crystallinity of P3ATs on the membrane gas selectivities and permeabilities. It is commonly accepted that the permeability of polymer membranes decreases with increasing degree of crystallinity of polymers as the transport of gas molecules occurs solely via the amorphous region.¹³⁻¹⁸ Homopolymers in film form a lamellar supramolecular organization, where the backbones are stacked via π -interactions and the flexible side chains are packed between the stacked backbones.¹⁹⁻²⁷ Random copolymers with a large difference in side chains, on the contrary, cannot form the above described supramolecular structure. By synthesizing both polymers, it was therefore possible to investigate the influence of the supramolecular organization, which is the driving force for the crystallization of rr-P3ATs, on the membrane permeabilities and selectivities while keeping chemical interactions between penetrant gas molecules and the polymer chains similar. Both the homopolymers and the copolymers were synthesized using the KCTCP to obtain well-defined rr-P3ATs.^{28,29} The obtained polymers were next cast in membranes to measure their gas transport properties. Positron annihilation lifetime spectroscopy (PALS) was used to measure the polymer free-volumes.

EXPERIMENTAL

Synthesis

Monomers

The precursor monomers, 2-bromo-5-iodo-3-hexylthiophene, 2-bromo-5-iodo-3-octylthiophene, 2-bromo-5-iodo-3-dodecylthiophene and 2-bromo-5-iodo-3-(2-ethylhexyl)thiophene were synthesized according to literature.²⁸ 2-Bromo-5-iodo-3-cyclohexylthiophene precursor monomer was synthesized as described elsewhere (Scheme 1).^{30,31}



Scheme 1. Synthesis of 2-bromo-5-iodo-3-cyclohexylthiophene. i, 1) Mg, 2) Ni(dppp)Cl₂, 3-bromothiophene; ii, N-bromosuccinimide; iii, I₂, phenyliododiacetate and the synthesis of the polymers.

Polymers

The homopolythiophenes and random copolythiophenes were synthesized following the general procedure (Scheme 1).²⁸ Four homopolythiophenes, poly(3-hexylthiophene) (P3HT), poly(3-octylthiophene) (P3OT), poly(3-(2-ethylhexyl)thiophene) (P3EHT) and poly(3-dodecylthiophene) (P3DDT) were prepared. In addition to this, three random

copolythiophenes, poly(3-(2-ethylhexyl)thiophene-co-3-cyclohexylthiophene)s (Cop25, Cop50 and Cop75) were synthesized. The number after the term Cop refers to the aimed monomer ratio percent of a 3-(2-ethylhexyl)thiophene monomer in the copolymer.

Characterization of polymers

Molar mass and structure of polymers

The obtained polymers were analyzed by gel permeation chromatography (GPC) to reveal the number average molar mass (\bar{M}_n) and dispersity (\mathcal{D}). The sample was prepared by dissolving approximately 2 mg of polymer in 2 ml of THF, the solution was passed through a filter of 0.20 μm pore diameter before injecting in the GPC device apparatus (Shimadzu 10 AVP). Prior to measurement, the device was calibrated using polystyrene standards and THF as eluent. ^1H NMR spectroscopy was used to record the polymer spectra in order to reveal their structures and the copolymer compositions. A Bruker Avance 400 MHz was used to record the ^1H NMR spectra of the polymers dissolved in CDCl_3 .

Thermal properties

Thermal properties of the polymers were measured by means of a TA instruments Q2000 differential scanning calorimeter (DSC). Samples of about 5 mg in closed TZero Aluminium Hermetic pans were scanned at a rate of 20 $^\circ\text{C}/\text{min}$ to record the thermograms.

Supramolecular organization

UV-vis spectra of the polymer solutions (CHCl_3) and films were recorded by a Varian Cary 400 apparatus. The films were prepared by spin coating the polymer solutions (2 wt%) on glass slides, which were stored in the dark to prevent photo-oxidation of the polymers.

Membrane preparation

All membranes were prepared by spin coating (600 rpm) the polymer solution (2 wt% in CHCl_3) on top of a porous crosslinked polyimide PI support.^{32,33} The spin coated layer was next sealed with a highly permeable polydimethylsiloxane (PDMS) layer.³⁴ In this way, the polymer selective layer was sandwiched between the two layers that provide respectively mechanical resistance and combined physical protection and defect-sealing. Since not all P3ATs could be processed into free-standing films with sufficient mechanical strength, the preparation of such thin film composite (TFC) film was preferred for all polymers. The thus obtained TFC-membranes were put in an oven at 140°C for 1 h to remove traces of solvents,³⁵ and to further crosslink the PDMS. The PDMS was prepared by dissolving RTV 615 (two component Kit, Momentive Performance Materials) in hexane (20 wt%) and heated at 60 °C for 1 h to initiate the crosslinking before spin coating.³⁴ The support was prepared via the process of phase inversion by deposition of a PI solution (Matrimid 15 wt%, *N*-methyl-2-pyrrolidone (NMP) 62.25 wt %, THF 20.75 wt% and 2wt% H) onto an NMP saturated non-woven PP/PE fabric (Novatex) by means of an automated casting knife (Braive Instruments, Belgium) set at 250 μm and 1.2 $\text{m}\cdot\text{min}^{-1}$.³⁶ After casting, the solvent was allowed to evaporate for 30 s and the membrane was immersed for 1 h in a deionized water bath for coagulation. To crosslink the support, it was immersed for 1 h in a methanol solution containing 5 wt% hexamethylenediamine, after which it was rinsed with methanol and then stored in methanol until further use.^{32,37}

Membrane characterization

Membrane morphology

The membrane internal microstructure was visualized by analyzing the membrane cross-section by means of a scanning electron microscope (SEM). Membrane cross-sections were

freeze fractured in liquid N₂ and sputter-coated with Au/Pd using a JEOL JFC-1300 auto fine coater prior to analysis. The apparatus used was a JEOL JSM-6010 LV microscope operated at an acceleration voltage of 10 kV.

Elemental analysis by EDX spectroscopy

Energy Dispersive X-ray spectra (EDS or EDX) of membrane cross-sections were recorded to trace the P3AT layer as it is the only membrane component possessing sulfur. Same samples prepared earlier for SEM experiments were re-used and analyzed using Phillips XL30 microscope equipped with a field emission gun and an EDAX EDX detector.

Polymer free-volumes

Positron annihilation lifetime spectroscopy (PALS) is a well-established tool to measure free-volumes in polymeric membranes.^{38,39} After thermalization, a positron and an electron can form a hydrogen-like element, the so-called positronium (Ps). It occurs either as *para*-positronium (*p*-Ps) in a spin-singlet state or as *ortho*-positronium (*o*-Ps) in a spin-triplet state. The positron of the *o*-Ps interacts with an electron of its surroundings and annihilates into two gamma-quanta with an average lifetime, the pick-off lifetime (τ), which can be measured and directly correlated to the free-volume hole size using Equation 1 according to the Tao-Eldrup model.^{40,41} From this equation, R represents the mean free-volume radius, and ΔR the electron layer thickness where there is a probability of finding the *o*-Ps. The latter, $\Delta R = 0.1656$ nm, is an empirical parameter which has been calculated from the materials with well-known free-volume hole size. λ equals 2 ns^{-1} and represents the spin-averages Ps annihilation rate in vacuum.

$$\tau = \frac{1}{\lambda} \left[1 - \frac{R}{R + \Delta R} + \frac{1}{2\pi} \sin\left(\frac{2\pi R}{R + \Delta R}\right) \right]^{-1}$$

Equation 1

The measurements were performed on the free-standing P3AT films prepared by solution casting. A polymer solution in CHCl_3 (2 wt%) was drop cast on glass slides and the solvent was slowly evaporated to yield the thick films. Samples underwent a vacuum treatment at 10^{-7} mbar for around 2 h before the PALS measurement was executed at the neutron induced positron source Munich (NEPOMUC) with the Pulsed Low-Energy Positron System (PLEPS), which produces a monochromatic positron beam of variable energy. This allows for depth-dependent PALS measurements, with a depth-resolution in the nanometer range.⁴² To make sure all positrons are implanted in the membrane, the used positron implantation energies were 2 and 4 keV, corresponding to, respectively, mean positron implantation depths of 97.82 nm and 320.16, when assuming a polymer density of 1 g/cm^3 . Even if the polymer density would differ from 1 by $\pm 0.5 \text{ g/cm}^3$, the membrane would still be probed at these implantation energies. However, as no significant differences were observed between different implantation depths, it can be concluded that all samples have a homogeneous free-volume structure throughout the film. The herein presented data were obtained at 2 keV. For these spectra 4 million counts were collected with a counting rate of about 10000 cts/s and a time resolution of about 250 ps. All spectra were evaluated with PALSfit.⁴³ The resolution function was determined by measuring p-doped SiC. The spectra were deconvoluted into either four lifetime components (*p*-Ps, free e^+ , *o*-Ps-short, *o*-Ps-long) or into 3 lifetime components (*p*-Ps, free e^+ , *o*-Ps, with a log-normal distribution on the latter), leading to good overall fit variances below 1.2.

Gas permeability and selectivity

A custom-built high-throughput gas separation (HTGSX) device apparatus described in detail elsewhere was used to analyze the gas transport properties of the P3AT membranes.⁴⁴ 16

different membrane coupons can be analyzed in parallel under mixed-gas conditions. Using a compact gas chromatograph (cGC, Interscience), the gas composition of the permeate was determined. An auxiliary cylinder with a constant volume connected to an MKS Baratron® pressure transducer enabled the calculation of the permeability through the membrane by monitoring the gas pressure in the cylinder using Equation 2.

$$P_i = 10^{10} \frac{y_i V L}{x_i p_{up} A T} \frac{dp}{dt}$$

Equation 2

where x_i and y_i are mole fractions of gas i in the upstream and downstream, respectively. V is the downstream volume in cm^3 , L is the membrane thickness (cm) and dp/dt refers to the increase pressure rate. A is the membrane area in cm^2 , T is the temperature in Kelvin and p_{up} the feed pressure in cmHg. The single gas selectivity α_{ij} between gas component i and j was determined by the ratio of their respective permeabilities ($\alpha_{ij} = \frac{P_i}{P_j}$) while the mixed gas selectivity was obtained by taking the mole fractions on downstream (y_i, y_j) and upstream (x_i, x_j) of the two gases as shown in Equation 3.

$$\alpha_{ij} = \frac{y_i/y_j}{x_i/x_j}$$

Equation 3

All measurements were done at 26 °C and the feed pressure was set at 3 bar.

X-ray diffraction experiments (XRD) were performed using a STOE Stadi P high-throughput powder XRD apparatus. The samples were measured in transmission mode using Cu K α X-rays ($\lambda = 1.5406 \text{ \AA}$).

RESULTS AND DISCUSSION

Synthesis and characterization of monomers and polymers

Synthesis of monomers and polymers

The structures of the precursor monomers and synthesized polymers were revealed by ^1H NMR. Four homopolythiophenes, **P3HT**, **P3OT**, **P3DDT** and **P3EHT**, and three poly(3-(2-ethylhexyl)thiophene-*co*-3-cyclohexylthiophene)s (**Cop25**, **Cop50** and **Cop75**) were successfully synthesized, whose structures are presented in Figure 1. In Table 1, the number average molar mass (\overline{M}_n) and the dispersity (\mathcal{D}) of the polymers are presented. The narrow molar mass distribution ($\mathcal{D} \leq 1.3$) for all P3ATs is in line with a controlled polymerization.^{45,46} Moreover, the analysis of the ^1H NMR spectra enabled to determine the monomer ratios in the random copolymers, by an integration of the monomer proton peaks at known chemical shifts, 7.08-6.99 ppm for 3-cyclohexylthiophene and 6.97-6.89 ppm for 3-(2-ethylhexyl)thiophene. From the integration, the percentage of 3-(2-ethylhexyl)thiophene monomer was found to be 26 % in **Cop25**, 52 % in **Cop50** and 75 % in **Cop75** (see SI).

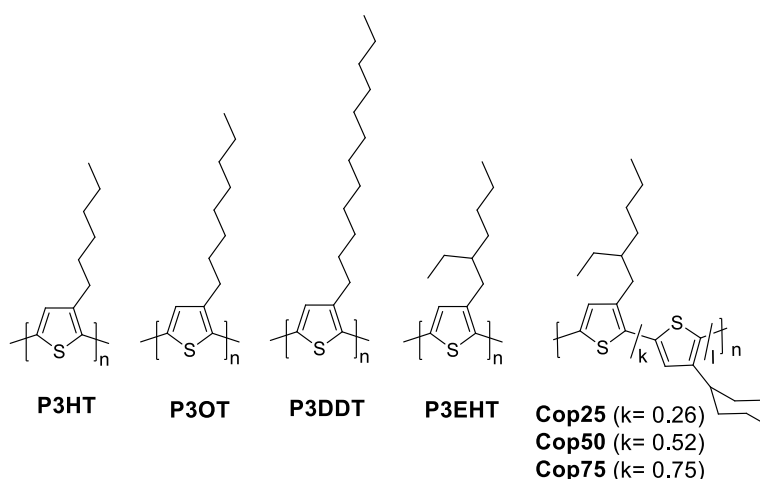


Figure 1. Structures of the synthesized polymers.

Table 1. Number average molar mass (\overline{M}_n) and dispersity (\mathcal{D}) of the polymers.

Polymer	\bar{M}_n (kg/mol)	\bar{D}
P3HT	39.4	1.2
P3OT	27.2	1.3
P3DDT	19.9	1.3
P3EHT	23.5	1.2
Cop25	6.5	1.3
Cop50	7.9	1.2
Cop75	9.2	1.1

Thermal properties of the polymers

The thermal properties of the homopolymers and the random copolymers were studied by DSC. From the thermograms (see SI), it is noticed that the homopolythiophenes, **P3HT**, **P3OT** and **P3DDT**, showed endothermic melting peaks at 239, 192 and 156 °C respectively. **P3EHT** instead showed two endothermic peaks at 70 and 89 °C with the first being the most intense. During a cooling cycle, the crystallization peaks were observed for **P3HT**, **P3OT** and **P3DDT** at 209 °C, 161 °C and 126 °C respectively. For **P3EHT**, no crystallization peak was detected, which could most likely be attributed to the slow crystallization.²² However, when the **P3EHT** was kept at 25 °C for 15 h and then re-heated, it showed again two endothermic peaks with similar intensity at 78 and 88 °C, strongly indicating that it had crystallized. From the DSC thermograms, it can thus be concluded that the homopolymers are semi-crystalline.^{21,22,47}

For the random copolymers, a melting peak is observed for **Cop75** at 213 °C and 67 °C for **Cop50**. **Cop25** instead did not show any melting peak. The latter polymer had a highest fraction of the bulky monomer, 3-cyclohexylthiophene, which could significantly hinder the crystallization. However, during the cooling, none of the copolymers crystallized, and the melting enthalpies of both **Cop50** and **Cop75** ($3.4 \pm 0.1 \text{ J g}^{-1}$) were inferior to that of the homopolymers ($14 \pm 1 \text{ J g}^{-1}$). The DSC results indicate that the copolymers have a much lower

degree of crystallinity than the homopolymers and that no crystallinity is present after melting.²¹ It was further noticed for the copolymers that both the melting temperatures and enthalpies decreased with increasing the content of the bulky 3-cyclohexylthiophene monomer. This can be justified by an inability of the bulky side chain to efficiently pack, as was anticipated.³¹ The thermograms of the copolymers can also be found in SI.

Supramolecular organization by UV-vis

UV-vis spectroscopy is widely used to study the supramolecular organization of P3ATs.^{21–23,25} The planarization of the polymer chains and intermolecular π - π stacking can be detected by the appearance of red-shifts and well-resolved shoulder absorption peak around 600 nm as compared to the spectra of polymer solutions.^{22,23,48} The UV-vis spectra of the polymer solutions and films (3 h and 1 week after spin coating) are presented in Figure 2. Barrer was the maximum value for the random copolymers, i.e. a difference of two orders of magnitude between the two polymer series. This difference is supposed to be way larger than the uncertainty on the exact determination of the thickness of the selective layer and of the exact permeation properties of the intruded layer. The homopolymers, having a clearly higher degree of crystallinity, are thus more permeable than the copolymers. This is an intriguing result to observe that the permeability increases with increasing degree of crystallinity. At the exception of one paper by Sawada *et al.*,⁵¹ it is commonly accepted that polymer crystallinity decreases the membrane permeability as the gas transport occurs solely through the amorphous region.^{13–18} Sawada *et al.* reported that the crystallinity of poly(lactic acid) (PLA) increased by thermal treatment (at and above 80 °C) of the PLA membrane. More interestingly, they indeed found that the permeability of the crystalline PLA membrane was higher than that of the amorphous. This was explained by linking the crystallinity (up to 20 %)

to the formation of a continuous space (larger than the gas molecule size) between the spherical discontinuous crystalline units and amorphous regions, by which gas molecules easily diffused. However, they noticed that at about 40 % crystallinity, continuous crystal branches appeared and the permeability dropped again. In the current study however, P3ATs, which have a different crystallization mechanism than common semi-crystalline polymers, were used. The crystalline part in semi-crystalline P3ATs consists of closely stacked thiophene backbones separated with a microphase of flexible alkyl side chains (Figure 4).^{19,20} The significantly higher permeability of semi-crystalline P3ATs must originate from the crystalline part. The closely stacked thiophene backbones cannot be the origin as they are too densely packed to even allow small gas molecules to pass.^{19,20} However, the flexible alkyl side chains form a very mobile microphase that can act as a pathway for the gas molecules, as illustrated in Figure 4. In amorphous P3ATs on the contrary, polymer chains are randomly entangled, which does not favor the formation of a pathway filled with flexible side chains. Thus, the higher degree of crystallinity leads to more of such pathways which enhance the permeation of gas molecules. This could explain why **P3HT**, the most crystalline (highest molar mass and shortest side chain) of the homopolymers,^{21,22,24,48} is the most permeable of all with a CO₂ permeability of 225 Barrer. This is the highest permeability ever reported with P3AT membranes.^{7,10,11} It is now clear that this is because previously reported P3ATs were regio-irregulars and could thus not form such nicely ordered semi-crystalline structures.

The selectivity data are presented in Table 2. For both mixed and single gas selectivities, three homopolymers out of four, i.e. **P3OT**, **P3DDT** and **P3EHT**, had higher selectivities, for both the CO₂/CH₄ and CO₂/N₂ gas pair, than the copolymers. **P3HT** with the lowest number of carbon atoms in the alkyl side chain, is an outlier in the homopolymer series with selectivities similar to those of the copolymers.

-From the UV-vis spectra, it is noticed that 3 hours after spin coating, the homopolymers showed red-shifts with shoulder absorption peaks around 600 nm, which remained after 1 week, strongly indicating the polymer aggregation.^{22,23} For the copolymers, on the contrary, there were no shoulders present, neither red-shifts, even after 1 week. These UV-vis results strongly indicate that upon spin coating, the way the P3AT is incorporated in the membrane, the homopolymers aggregate and form a supramolecular structure, while the copolymers cannot. This is in line with what was observed in the DSC measurements. The copolymers did not show crystallization peaks after melting, nor do they show any sign of organization after spin coating. Both DSC and UV-vis results thus point in a same direction and indicate that the copolymers do not organize as the homopolymers do. This was confirmed by X-ray diffraction experiments. (Figure SI19).

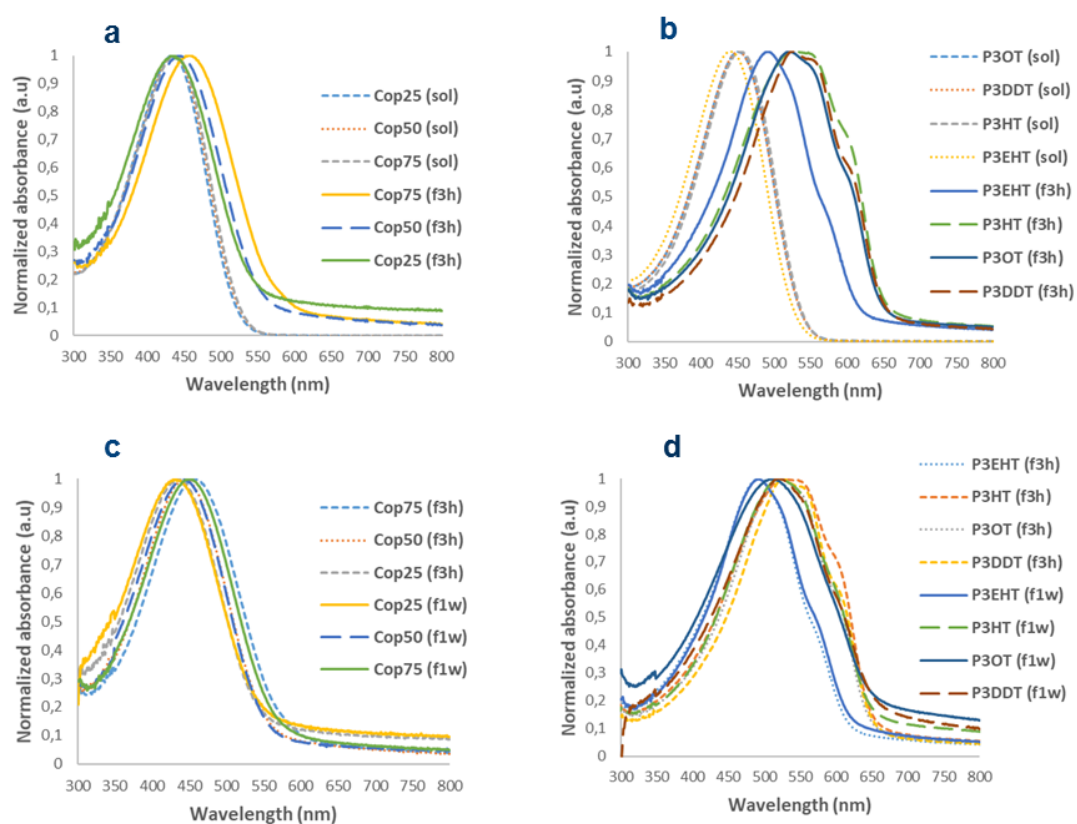


Figure 2. UV-vis patterns of **a**, copolymers in solution (sol) and copolymer films 3h after spin

coating (f3h); b, homopolymers in solution and films 3h after spin coating; c, copolymers films 3h and 1 week after casting (f1w); d, homopolymers films 3h and 1 week after spin coating

Membrane characterization

SEM-EDX

Analysis of the SEM images of the membrane cross-sections revealed the formation of a P3AT dense layer between the PDMS sealing layer and the porous PI support (Figure 3). In addition, it was noticed that the P3AT solution had intruded in the porous structure of PI support, forming an additional selective phase with mixed composition. This was supported by EDX analysis of the intruded phase in which sulfur was detected (Figure 3). This extra selective layer was therefore taken into account in the measurement of the total thickness of the selective layer. It was assumed that the intrusions in the support resulted in an average volume fraction of 10 % of the P3AT (based on TEM cross-section image of such a support).⁴⁹ The thickness of the dense layer was determined from SEM cross-section images. The overall permeability of the composite intruded layer was determined and de-convoluted based on a linear combination of the pure matrimid (PI) and P3AT permeabilities using the above mentioned volume fraction. For matrimid, literature permeability values were taken.⁵⁰ Even though the intruded P3AT layers could have different properties than the P3AT bulk phases with respect to *e.g.* swelling and chain mobility, they were thus considered together with the actual P3AT dense layer on top, as one homogeneous thick layer.

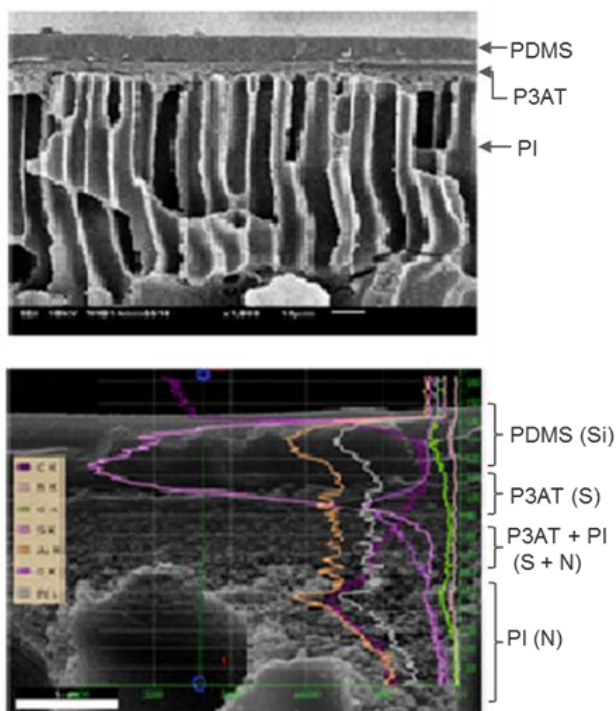


Figure 3. SEM image (up) and EDX line scan with the most characteristic chemical elements per layer shown in brackets of the P3HT membrane cross-section (bottom image).

Permeability and selectivity results

The CO₂ permeability data (Table 2) reveal that the homopolymers were much more permeable than the copolymers. A maximum CO₂ permeability of up to 225 Barrer was recorded for the homopolymers, while 2 Barrer was the maximum value for the random copolymers, i.e. a difference of two orders of magnitude between the two polymer series. This difference is supposed to be way larger than the uncertainty on the exact determination of the thickness of the selective layer and of the exact permeation properties of the intruded layer. The homopolymers, having a clearly higher degree of crystallinity, are thus more permeable than the copolymers. This is an intriguing result to observe that the permeability increases with increasing degree of crystallinity. At the exception of one paper by Sawada *et al.*,⁵¹ it is commonly accepted that polymer crystallinity decreases the membrane permeability

as the gas transport occurs solely through the amorphous region.¹³⁻¹⁸ Sawada *et al.* reported that the crystallinity of poly(lactic acid) (PLA) increased by thermal treatment (at and above 80 °C) of the PLA membrane. More interestingly, they indeed found that the permeability of the crystalline PLA membrane was higher than that of the amorphous. This was explained by linking the crystallinity (up to 20 %) to the formation of a continuous space (larger than the gas molecule size) between the spherical discontinuous crystalline units and amorphous regions, by which gas molecules easily diffused. However, they noticed that at about 40 % crystallinity, continuous crystal branches appeared and the permeability dropped again. In the current study however, P3ATs, which have a different crystallization mechanism than common semi-crystalline polymers, were used. The crystalline part in semi-crystalline P3ATs consists of closely stacked thiophene backbones separated with a microphase of flexible alkyl side chains (Figure 4).^{19,20} The significantly higher permeability of semi-crystalline P3ATs must originate from the crystalline part. The closely stacked thiophene backbones cannot be the origin as they are too densely packed to even allow small gas molecules to pass.^{19,20} However, the flexible alkyl side chains form a very mobile microphase that can act as a pathway for the gas molecules, as illustrated in Figure 4. In amorphous P3ATs on the contrary, polymer chains are randomly entangled, which does not favor the formation of a pathway filled with flexible side chains. Thus, the higher degree of crystallinity leads to more of such pathways which enhance the permeation of gas molecules. This could explain why **P3HT**, the most crystalline (highest molar mass and shortest side chain) of the homopolymers,^{21,22,24,48} is the most permeable of all with a CO₂ permeability of 225 Barrer. This is the highest permeability ever reported with P3AT membranes.^{7,10,11} It is now clear that this is because previously reported P3ATs were regio-irregulars and could thus not form such nicely ordered semi-crystalline structures.

The selectivity data are presented in Table 2. For both mixed and single gas selectivities, three homopolymers out of four, i.e. **P3OT**, **P3DDT** and **P3EHT**, had higher selectivities, for both the CO₂/CH₄ and CO₂/N₂ gas pair, than the copolymers. **P3HT** with the lowest number of carbon atoms in the alkyl side chain, is an outlier in the homopolymer series with selectivities similar to those of the copolymers.

Table 2. Permeability and selectivity results. Values shown are the average of 3 replicates, except for P3OT and P3DDT, where only one measurement could be executed ().*

Polymer	P_{CO_2} (Barrer)	Mixed gas	Single gas	
		α_{CO_2/CH_4}	P_{CO_2}/P_{CH_4}	P_{CO_2}/P_{N_2}
P3HT	225 ± 3	10 ± 1	13 ± 2	29 ± 2
P3OT*	81.5	24.5	38.9	46.7
P3DDT*	142	23.7	24.7	48.2
P3EHT	84 ± 2	25.4 ± 4.0	38 ± 12	44 ± 5
Cop25	1.20 ± 0.04	13 ± 1	11 ± 1	18 ± 2
Cop50	1.3 ± 0.1	12 ± 2	11 ± 1	17 ± 2
Cop75	2.1 ± 0.1	10 ± 1	13.8	16 ± 1

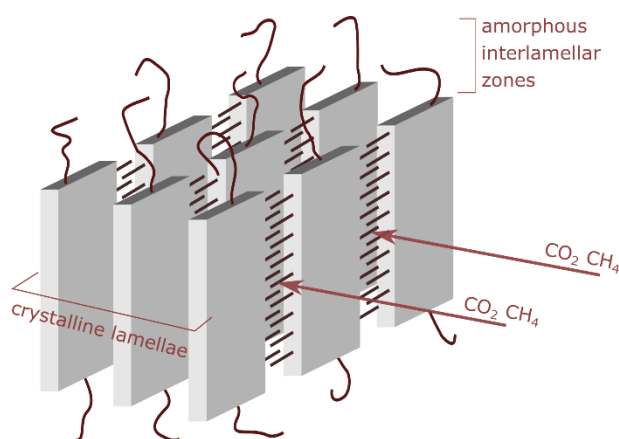


Figure 4. Schematic representation of the organization of the semi-crystalline structure of rr-P3AT, with crystalline regions formed by stacked backbones and amorphous regions, formed

by entangled chains. Gas transport is believed to occur through the microphases, formed by the flexible side chains of the backbone. Figure inspired from ¹⁹.

PALS

The analysis of the PALS spectra of all samples with the simplest multi-exponential model required four lifetime components (p-Ps, free e⁺, o-Ps-short and o-Ps-long) to adequately describe the data, corresponding to two different average free volumes (Figure 15 and 16 in SI). Alternatively, the data could be described with three lifetime components (p-Ps, free e⁺, o-Ps), with a broad log-normal distribution on the o-Ps species (Figure 17 and 18 in SI). Additional information is required to differentiate between both models as they both have similar and good fit variances. The overall conclusion of both models is nevertheless the same: the homopolymers contain larger free-volume elements than the copolymers. In the four lifetime fit, no significant differences were observed for the o-Ps-short lifetime. However, the lifetime of the long o-Ps species was significantly longer for all homopolymers (Figure 5). Also, the intensities of the o-Ps-long lifetime (except for P3EHT) are higher than those of the copolymers (Figure 16 in SI). These findings suggest that the homopolymers contain more and larger free-volume elements than the copolymers. The PALS results are thus readily consistent with the membrane separation data, where the homopolymers obtained significantly higher gas permeabilities than the copolymers.

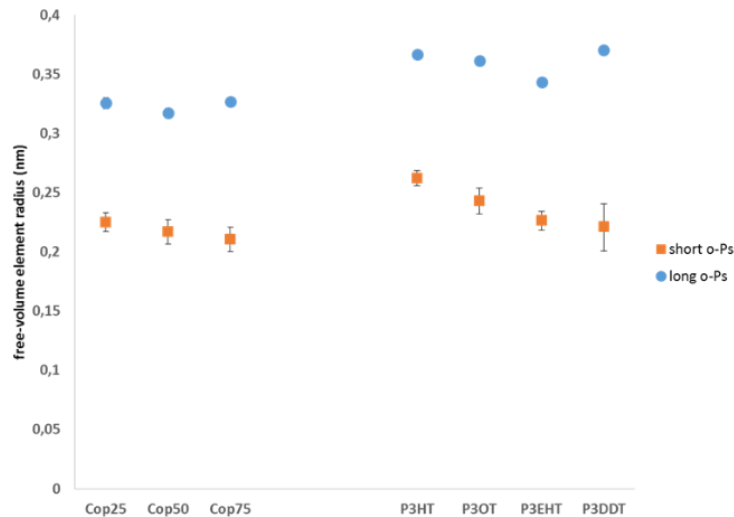


Figure 5. Average free-volume element radii of the homo- and copolymers, based on the short-living and long-living o-Ps. The results were obtained via a multi-exponential model with four lifetime components.

On the other hand, when comparing the different homopolymers, not such big differences in free-volume element radii are observed. In the crystalline part, the distance between the stacked piles of thiophene backbones, which depends on the length of the side chain,²⁴ is significantly larger for **P3DDT** than for **P3HT**. As a consequence, if PALS would detect free-volume elements in the crystalline part (*i.e.* in the alkyl phase, where the gas permeation occurs), the free-volume elements for **P3HT** and **P3DDT** should be significantly different. Knowing that these zones which are filled up by the alkyl side chains of the monomers behave like alkanes, it seems indeed acceptable that PALS does not manage to probe free volumes in such highly mobile phase. This is in agreement with the overall accepted vision that o-Ps annihilation is sensitive to local, microscopic properties rather than to the bulk properties of the polymer.⁵² In conclusion, the free-volume elements probed with PALS are solely situated in the amorphous region, which is not the dominant part of the membrane for gas transport of the homopolymers. In the same manner, it is not possible to relate the difference in

selectivity of the membranes to the size of the free-volume elements. As a consequence, PALS is not able to identify whether solubility selectivity or diffusion selectivity dominates.

CONCLUSIONS

To study the influence of the supramolecular organization and crystallinity of rr-P3ATs on the membrane gas transport properties, two series of rr-P3ATs, homopolymers and random copolymers, were synthesized. After spin coating, the homopolymers aggregated in supramolecular structures in contrast with the random copolymers. The gas transport measurements revealed that the permeabilities of the homopolymers were almost two orders of magnitude higher than those of the copolymers. The higher permeability of the homopolymers was attributed to the formation of a microphase of flexible side chains which acts as a pathway for the gas molecules. Reported polythiophene membranes thus form a unique system where a higher degree of crystallinity leads to higher permeabilities.

AUTHOR INFORMATION

Corresponding author

*E-mail guy.koeckelberghs@kuleuven.be (G.K.).

Notes

The authors declare no competing financial interest.

ACKNOWLEDGEMENTS

We are grateful to the IDO/Research Fund KU Leuven for financial support. C.V.G. acknowledges the IWT for a doctoral fellowship. R.V. thanks Research Foundation-Flanders (FWO) for a SB-PhD fellowship (1S00917N). PALS results are based upon experiments

performed at the NEPOMUC PLEPS instrument operated by FRM-II at the Heinz Maier-Leibnitz Zentrum (MLZ), Garching, Germany.

ASSOCIATED CONTENT

Supporting Information. ^1H NMR, DSC, PALS and XRD of the polymers.

REFERENCES

- (1) Galizia, M.; Chi, W. S.; Smith, Z. P.; Merkel, T. C.; Baker, R. W.; Freeman, B. D. 50th Anniversary Perspective: Polymers and Mixed Matrix Membranes for Gas and Vapor Separation: A Review and Prospective Opportunities. *Macromolecules* **2017**, *50* (20), 7809–7843.
- (2) Baker, R. W. Future Directions of Membrane Gas Separation Technology. *Industrial and Engineering Chemistry Research*. 2002, pp 1393–1411.
- (3) Mulder, M. *Basic Principles of Membrane Technology*; Kluwer Academic, 1996; Vol. 72.
- (4) Baker, R. W.; Low, B. T. Gas Separation Membrane Materials: A Perspective. *Macromolecules* **2014**, *47* (20), 6999–7013.
- (5) Li, C.; Li, P.; Chen, L.; Briggs, M. E.; Liu, M.; Chen, K.; Shi, X.; Han, D.; Ren, S. Pyrene-Cored Covalent Organic Polymers by Thiophene-Based Isomers, Their Gas Adsorption, and Photophysical Properties. *J. Polym. Sci. Part A Polym. Chem.* **2017**, *55* (14), 2383–2389.
- (6) Wang, Z.; Liu, J.; Fu, Y.; Liu, C.; Pan, C.; Liu, Z.; Yu, G. Fabrication of Conjugated Microporous Polytriazine Nanotubes and Nanospheres for Highly Selective CO₂ capture. *Chem. Commun.* **2017**, *53* (29), 4128–4131.

- (7) Pellegrino, J. The Use of Conducting Polymers in Membrane-Based Separations: A Review and Recent Developments. In *Annals of the New York Academy of Sciences*; 2003; Vol. 984, pp 289–305.
- (8) Illing, G.; Hellgardt, K.; Wakeman, R. J.; Jungbauer, A. Preparation and Characterisation of Polyaniline Based Membranes for Gas Separation. *J. Memb. Sci.* **2001**, *184* (1), 69–78.
- (9) Liang, W.; Martin, C. R. Gas Transport in Electronically Conductive Polymers. *Chem. Mater.* **1991**, *3* (3), 390–391.
- (10) Reid, B. D.; Ebron, V. H. M.; Musselman, I. H.; Ferraris, J. P.; Balkus, K. J. Enhanced Gas Selectivity in Thin Film Composite Membranes of poly(3-(2-Acetoxyethyl)thiophene). *J. Memb. Sci.* **2002**, *195* (2), 181–192.
- (11) Musselman, I. H.; Li, L.; Washmon, L.; Varadarajan, D.; Riley, S. J.; Hmyene, M.; Ferraris, J. P.; Balkus, K. J. Poly(3-Dodecylthiophene) Membranes for Gas Separations. *J. Memb. Sci.* **1999**, *152* (1), 1–18.
- (12) Anjum, M. W. Polymer-Based Membranes For CO₂ Separations. *PhD thesis* **2015**, 95–110.
- (13) Bitter, J. G. A. Effect of Crystallinity and Swelling on the. *Desalination* **1984**, *51* (1), 19–35.
- (14) Lin, H.; Freeman, B. D. Gas Solubility, Diffusivity and Permeability in Poly(ethylene Oxide). *J. Memb. Sci.* **2004**, *239* (1), 105–117.
- (15) Yave, W.; Car, A.; Funari, S. S.; Nunes, S. P.; Peinemann, K. V. CO₂-Philic Polymer Membrane with Extremely High Separation Performance. *Macromolecules* **2010**, *43*

- (1), 326–333.
- (16) Xue, B.; Gao, L.; Jiang, H.; Geng, Z.; Guan, S.; Wang, Y.; Liu, Z.; Jiang, L. High Flux CO₂transporting Nanochannel Fabricated by the Self-Assembly of a Linear-Brush Block Copolymer. *J. Mater. Chem. A* **2013**, *1* (28), 8097–8100.
- (17) Car, A.; Stropnik, C.; Yave, W.; Peinemann, K. V. Tailor-Made Polymeric Membranes Based on Segmented Block Copolymers for CO₂ Separation. *Adv. Funct. Mater.* **2008**, *18* (18), 2815–2823.
- (18) Metz, S. J.; Mulder, M. H. V.; Wessling, M. Gas-Permeation Properties of Poly(ethylene Oxide) Poly(butylene Terephthalate) Block Copolymers. *Macromolecules* **2004**, *37* (12), 4590–4597.
- (19) Brinkmann, M.; Rannou, P. Effect of Molecular Weight on the Structure and Morphology of Oriented Thin Films of Regioregular poly(3-Hexylthiophene) Grown by Directional Epitaxial Solidification. *Adv. Funct. Mater.* **2007**, *17* (1), 101–108.
- (20) Yamamoto, T.; Komarudin, D.; Arai, M.; Lee, B. L.; Suganuma, H.; Asakawa, N.; Inoue, Y.; Kubota, K.; Sasaki, S.; Fukuda, T.; Matsuda, H. Extensive Studies on π -Stacking of poly(3-Alkylthiophene-2,5-Diyl)s and poly(4-Alkylthiazole-2,5-Diyl)s by Optical Spectroscopy, NMR Analysis, Light Scattering Analysis, and X-Ray Crystallography. *J. Am. Chem. Soc.* **1998**, *120* (9), 2047–2058.
- (21) Zhang, Y.; Tajima, K.; Hashimoto, K. Nanostructure Formation in poly(3-Hexylthiophene-Block- 3-(2-Ethylhexyl)thiophene)s. *Macromolecules* **2009**, *42* (18), 7008–7015.
- (22) Boudouris, B. W.; Ho, V.; Jimison, L. H.; Toney, M. F.; Salleo, A.; Segalman, R. A. Real-

- Time Observation of Poly (3-Alkylthiophene) Crystallization and Correlation with Transient Optoelectronic Properties. *Macromolecules* **2011**, *44* (17), 6653–6658.
- (23) Xu, W.; Li, L.; Tang, H.; Li, H.; Zhao, X.; Yang, X. Solvent-Induced Crystallization of poly(3-Dodecylthiophene): Morphology and Kinetics. *J. Phys. Chem. B* **2011**, *115* (20), 6412–6420.
- (24) Causin, V.; Marega, C.; Marigo, A.; Valentini, L.; Kenny, J. M. Crystallization and Melting Behavior of Poly(3-Butylthiophene), Poly(3-Octylthiophene), and Poly(3-Dodecylthiophene). *Macromolecules* **2005**, *38* (2), 409–415.
- (25) Yamamoto, T.; Komarudin, D.; Arai, M.; Lee, B. L.; Suganuma, H.; Asakawa, N.; Inoue, Y.; Kubota, K.; Sasaki, S.; Fukuda, T.; Matsuda, H. Extensive Studies on π -Stacking of poly(3-Alkylthiophene-2,5-Diyl)s and poly(4-Alkylthiazole-2,5-Diyl)s by Optical Spectroscopy, NMR Analysis, Light Scattering Analysis, and X-Ray Crystallography. *J. Am. Chem. Soc.* **1998**, *120* (9), 2047–2058.
- (26) Ouhib, F.; Desbief, S.; Lazzaroni, R.; De Winter, J.; Gerbaux, P.; Jérôme, C.; Detrembleur, C. Thermally Induced Coupling of Poly(thiophene)-Based Block Copolymers Prepared by Grignard Metathesis Polymerization: A Straightforward Route toward Highly Regioregular Multiblock Conjugated Copolymers. *Macromolecules* **2012**, *45* (17), 6796–6806.
- (27) Peeters, H.; Couturon, P.; Vandeleene, S.; Moerman, D.; Leclère, P.; Lazzaroni, R.; Cat, I. De; Feyter, S. De; Koeckelberghs, G. Influence of the Regioregularity on the Chiral Supramolecular Organization of poly(3-Alkylsulfanylthiophene)s. *RSC Adv.* **2013**, *3* (10), 3342–3351.

- (28) Verswyvel, M.; Monnaie, F.; Koeckelberghs, G. AB Block copoly(3-Alkylthiophenes): Synthesis and Chiroptical Behavior. *Macromolecules* **2011**, *44* (24), 9489–9498.
- (29) Verheyen, L.; Leysen, P.; Van Den Eede, M. P.; Ceunen, W.; Hardeman, T.; Koeckelberghs, G. Advances in the Controlled Polymerization of Conjugated Polymers. *Polymer*. Elsevier Ltd January 2017, pp 521–546.
- (30) Berggren, M.; Gustafsson, G.; Inganäs, O.; Andersson, M. R.; Wennerström, O.; Hjertberg, T. Green Electroluminescence in Poly-(3-cyclohexylthiophene) Light-emitting Diodes. *Adv. Mater.* **1994**, *6* (6), 488–490.
- (31) Andersson, M. R.; Berggren, M.; Inganäs, O.; Gustafsson, G.; Gustafsson-Carlberg, J. C.; Seise, D.; Hjertberg, T.; Wennerström, O. Electroluminescence from Substituted Poly(thiophenes): From Blue to Near-Infrared. *Macromolecules* **1995**, *28* (22), 7525–7529.
- (32) Vanherck, K.; Vandezande, P.; Aldea, S. O.; Vankelecom, I. F. J. Cross-Linked Polyimide Membranes for Solvent Resistant Nanofiltration in Aprotic Solvents. *J. Memb. Sci.* **2008**, *320* (1–2), 468–476.
- (33) Vanherck, K.; Koeckelberghs, G.; Vankelecom, I. F. J. Crosslinking Polyimides for Membrane Applications: A Review. *Prog. Polym. Sci.* **2013**, *38* (6), 874–896.
- (34) Basu, S.; Cano-Odena, A.; Vankelecom, I. F. J. MOF-Containing Mixed-Matrix Membranes for CO₂/CH₄ and CO₂/N₂ Binary Gas Mixture Separations. *Sep. Purif. Technol.* **2011**, *81* (1), 31–40.
- (35) Yampolskii, Y.; Alentiev, A.; Bondarenko, G.; Kostina, Y.; Heuchel, M. Intermolecular Interactions: New Way to Govern Transport Properties of Membrane Materials. *Ind.*

Eng. Chem. Res. **2010**, *49* (23), 12031–12037.

- (36) Hořda, A. K.; Vankelecom, I. F. J. Understanding and Guiding the Phase Inversion Process for Synthesis of Solvent Resistant Nanofiltration Membranes. *J. Appl. Polym. Sci.* **2015**, *132* (27), 42130.
- (37) Vanherck, K.; Cano-Odena, A.; Koeckelberghe, G.; Dedroog, T.; Vankelecom, I. A Simplified Diamine Crosslinking Method for PI Nanofiltration Membranes. *J. Memb. Sci.* **2010**, *353* (1–2), 135–143.
- (38) Jansen, J. C.; MacChione, M.; Tocci, E.; De Lorenzo, L.; Yampolskii, Y. P.; Sanfirova, O.; Shantarovich, V. P.; Hofmann, D.; Drioli, E. Comparative Study of Different Probing Techniques for the Analysis of the Free Volume Distribution in Amorphous Glassy Perfluoropolymers. *Macromolecules* **2009**, *42* (19), 7589–7604.
- (39) Verbeke, R.; Gómez, V.; Koschine, T.; Eyley, S.; Szymczyk, A.; Dickmann, M.; Stimpel-Lindner, T.; Egger, W.; Thielemans, W.; Vankelecom, I. F. J. Real-Scale Chlorination at pH4 of BW30 TFC Membranes and Their Physicochemical Characterization. *J. Memb. Sci.* **2018**, *551* (September 2017), 123–135.
- (40) Eldrup, M.; Lightbody, D.; Sherwood, J. N. The Temperature Dependence of Positron Lifetimes in Solid Pivalic Acid. *Chem. Phys.* **1981**, *63* (1–2), 51–58.
- (41) Tao, S. J. Positronium Annihilation in Molecular Substances. *J. Chem. Phys.* **1972**, *56* (11), 5499–5510.
- (42) Willutzki, P.; Stormer, J.; Kogel, G.; Reiner, M.; Pikart, P.; Hugenschmidt, C.; Wagner, A.; Butterling, M.; Fiedler, F.; Ravelli, L.; Löwe, B.; Egger, W.; Kögel, G.; Sperr, P.; Dollinger, G. Geant4 Simulation of the Effect of Backscattered Positrons on the

- Lifetime Spectra of PLEPS An Improved Pulsed Low-Energy Positron System Position-Resolved Positron Annihilation Lifetime Spectroscopy Geant4 Simulation of the Effect of Backscattered Positron. *J. Phys. Conf. Ser* **2013**, *443*, 1–4.
- (43) Mostgaard, M.; Kirkegaard, P.; Olsen, J. V; Eldrup, M. *PALSfit3: A Software Package for Analysing Positron Lifetime Spectra*; 2017; Vol. 13.
- (44) Khan, A. L.; Basu, S.; Cano-Odena, A.; Vankelecom, I. F. J. Novel High Throughput Equipment for Membrane-Based Gas Separations. *J. Memb. Sci.* **2010**, *354* (1–2), 32–39.
- (45) Miyakoshi, R.; Yokoyama, A.; Yokozawa, T. Catalyst-Transfer Polycondensation. Mechanism of Ni-Catalyzed Chain-Growth Polymerization Leading to Well-Defined poly(3-Hexylthiophene). *J. Am. Chem. Soc.* **2005**, *127* (49), 17542–17547.
- (46) Iovu, M. C.; Sheina, E. E.; Gil, R. R.; McCullough, R. D. Experimental Evidence for the Quasi-“living” nature of the Grignard Metathesis Method for the Synthesis of Regioregular poly(S-Alkylthiophenes). *Macromolecules* **2005**, *38* (21), 8649–8656.
- (47) Malik, S.; Nandi, A. K. Crystallization Mechanism of Regioregular poly(3-Alkyl Thiophene)s. *J. Polym. Sci. Part B Polym. Phys.* **2002**, *40* (18), 2073–2085.
- (48) Shen, X.; Hu, W.; Russell, T. P. Measuring the Degree of Crystallinity in Semicrystalline Regioregular poly(3-Hexylthiophene). *Macromolecules* **2016**, *49* (12), 4501–4509.
- (49) Hermans, S.; Dom, E.; Mariën, H.; Koeckelberghs, G.; Vankelecom, I. F. J. Efficient Synthesis of Interfacially Polymerized Membranes for Solvent Resistant Nanofiltration. *J. Memb. Sci.* **2015**, *476*, 356–363.
- (50) Tin, P. S.; Chung, T. S.; Liu, Y.; Wang, R.; Liu, S. L.; Pramoda, K. P. Effects of Cross-

Linking Modification on Gas Separation Performance of Matrimid Membranes. *J.*

Memb. Sci. **2003**, 225 (1–2), 77–90.

(51) Sawada, H.; Takahashi, Y.; Miyata, S.; Kanehashi, S.; Sato, S.; Nagai, K. Gas Transport

Properties and Crystalline Structures of Poly(lactic Acid) Membranes. *Trans. Mater.*

Res. Soc. Japan **2010**, 35 (2), 241–246.

(52) Dlubek, G.; Bamford, D.; Wilkinson, I.; Borisch, K.; Alam, M. A.; Tschierske, C.

Investigation of Thermotropic Phase Transitions in a Triple Chain Amphiphile Forming

Hexagonal Columnar and Inverse Micellar Cubic Mesophases: A Positron Annihilation

Lifetime Study. *Liq. Cryst.* **1999**, 26 (6), 863–870.

FOR TABLE OF CONTENTS ONLY

Increasing membrane permeability by increasing the polymer crystallinity: the unique case of polythiophenes

Mikael Monga Mulunda, Cédric van Goethem, Rhea Verbeke, Tönjes Koschine, Michael Wübbenhorst, Zidan Zhang, Erik Nies, Marcel Dickmann, Werner Egger, Ivo F.J. Vankelecom, and Guy Koeckelberghs

